Available online at www.sciencedirect.com
SCIENCE DIRECT®
Polymer 44 (2003) 5759–5769
polymer
www.elsevier.com/locate/polymer

Shear induced crystallization in poly(ε-caprolactone): effect of shear rate

D. Lellinger[c], G. Floudas[a,b,*], I. Alig[c,*]

[a]*Department of Physics, University of Ioannina, P.O. Box 1186, 451 10 Ioannina, Greece*
[b]*Foundation for Research and Technology-Hellas (FO.R.T.H), Biomedical Research Institute (B.R.I.), Ioannina, Greece*
[c]*Deutsches Kunststoff-Institut, Schlossgartenstrasse 6, D-64289 Darmstadt, Germany*

Received 18 February 2003; received in revised form 15 July 2003; accepted 15 July 2003

Abstract

We have studied the effect of shear rate on the very early stages of poly(ε-caprolactone) crystallization with in situ rheology and ex situ optical microscopy. The effect of shear rate is mainly to increase the nucleation density and to speed-up the crystallization process. Thermally-induced crystallization is separated from strain-induced crystallization allowing the construction of a 'master curve' indicating that the system obeys the shear rate—temperature—superposition. It was found that the free enthalpy difference in the melt $G_m(\dot{\gamma}, T) - G_m(\dot{\gamma} = 0, T)$ increases with the shear rate ($\dot{\gamma}$) that can be qualitatively rationalized by the reduced entropy of the melt prior to crystallization.

Keywords: Crystallization; Shear; Poly(ε-caprolactone)

1. Introduction

The problem of strain-induced crystallization is known since the crystallization of rubber. It is known that the morphology of the crystal obtained from a strained liquid is very different from that obtained from a fully relaxed liquid. For example, the isotropically grown spherulites in the latter case are replaced by row nuclei epitaxially overgrown by densely packed or irregularly spaced lamellae (shish-kebabs), giving rise to highly anisotropic structures [1,2]. Shear-induced crystallization is of great technological importance in all fabrication processes such as injection moulding, extrusion, fiber spinning and film blowing. Ideally one would like to know how external shear influence: the entropy and enthalpy of the melt state, the equilibrium melting temperature, the nucleation density, the nucleation and growth rates, the morphology from the primary nuclei to the superstructure, etc. At present, a satisfactory knowledge of the above thermodynamic quantities and parameters remains an illusion and a challenge to both theoreticians and experimentalists. A better understanding of some of the above parameters involved in shear-induced crystallization may permit the design of improved fabrication methods. There are, however, some practical problems to be solved: fabrication methods are using deformation and cooling rates much higher than those achievable by a laboratory rheometer.

Some progress has recently been made in this direction by employing the higher stress levels encountered in industrial processes [3]. Of particular importance are experimental attempts aiming to separate the shear-induced nucleation from the subsequent growth. One approach is by applying shear in the melt state following by a quench to the final crystallization temperature [4]. This treatment results in the formation of precursors in the form of liquid fibrils. Another approach is by applying short-time shearing at low degrees of supercooling where the shear-induced nucleation is followed by crystal growth after the cessation of flow [5,6]. In the latter case, intensive shearing resulted in nuclei growing into thread-like precursors. There exist also some recent theoretical attempts to quantify the effect of flow on polymer crystallization [7,8]. From the experimental point of view, shear-induced crystallization has been studied on high density polyethylene (HDPE) [9,10], poly(1-butene) (PB-1) [11], polypropylene (PP) [12–17], poly(ε-caprolactone) (PCL) [18], poly(ether ether ketone) (PEEK) [19] and poly(ethylene oxide) (PEO) [18,20]. Planar, rotary and couette shear devices have been employed together with a laboratory extruder [14,15]. With a few exceptions [3,14,15]

* Corresponding authors. Tel.: +30-2651098564; fax: +30-2651098693.
E-mail address: gfloudas@cc.uoi.gr (G. Floudas).

0032-3861/$ - see front matter © 2003 Elsevier Ltd. All rights reserved.
doi:10.1016/S0032-3861(03)00633-5

the deformation rates were much smaller than the ones corresponding to industrial conditions. In the vast majority of cases it was found that the shear rate affects mainly the nucleation rate and speed-up the crystallization process. Furthermore, a recent rheological study [21] of shear induced crystallization in isotactic polypropylene has shown that both the shear rate and the total shearing time can influence the crystallization process and the highest effect was produced for combinations of high shear rates and short shearing times. Despite these effects, the way the shear rate enters the thermodynamics is largely unexplored.

Herein we explore the initial nuclei formation under low shear rates in a poly(ε-caprolactone) (PCL) with a number averaged molecular weight of 8×10^4 using in situ rheology and ex situ optical microscopy. PCL was employed in our recent study of birefringence and dichroism evolution during crystallization [22]. An increasing volume fraction of axialites at early times and crystal branching and randomization in orientation at later times were found to control the signal from optical rheometry. In addition, it was shown that decreasing temperature and increasing shear rate affect mainly the nucleation density. In the present study optical microscopy was also employed to obtain the nucleation density for the different shear rates as well as the growth rate for the unstrained sample. The nucleation density was found to be strongly enhanced by the shear. From the rheological experiments in the present study it was found that an increase in the shear rate speed-up the crystallization process. Assuming that the growth rate at a given shear rate can be separated in a factor depending only upon temperature and a second term which contains all the shear rate dependence, i.e. $R_g(T, \dot{\gamma}) = R_g(T, \dot{\gamma} = 0)f(\dot{\gamma})$, we are able to calculate the reduction of the Gibbs free energy barrier $\Delta g^*(T, \dot{\gamma})$ to form oriented and elongated chain segments or (secondary) nuclei of critical size by the shear flow. The shear contribution to the free enthalpy difference in the melt $G_m(\dot{\gamma}, T) - G_m(\dot{\gamma} = 0, T)$, was found to increase with the shear rate. We attribute this increase to the reduction of the melt state entropy prior to crystallization. Moreover, the system obeys the shear rate—temperature—superposition principle, at least over the small range of temperatures and shear rates investigated, implying the existence of a unique scaling of the characteristic crystallization times with decreasing temperatures and increasing shear rates.

The paper is organized as follows: in the first part, we report on the thermal induced crystallization (limit of very low shear rates). The analysis of the crystallization under such conditions is the basis for interpreting the results of the subsequent experiments. In addition, different morphological models are applied to describe the evolution of the viscoelastic properties. In the second part, the influence of shear flow on the initial nuclei formation under low shear rates was investigated in steady shear experiments and discussed in terms of entropy changes in the melt before crystallization. In the third part, we make use of the combined information from the thermal and shear induced crystallization suggesting a 'master curve' construction that takes into account both effects.

2. Experimental section

The PCL homopolymer (Aldrich) was synthesized by anionic polymerization following standard procedures and kindly provided by Dr G. Reiter (CNRS, Mulhouse). The sample had a number averaged molecular weight of 8×10^4.

2.1. Rheology

An advanced rheometric expansion system (ARES) equipped with a force-rebalanced transducer was used. Both oscillatory shear and steady shear experiments have been performed. The oscillatory shear experiment was made with a parallel plate geometry (sample thickness of about 1 mm) with a frequency of 1 rad/s and a small strain amplitude (the maximum strain amplitude was 4%) so that to avoid any shear-induced orientation. The experiments consisted of T-jumps from an initial temperature of 353 K located above the equilibrium melting point (see below) to different final crystallization temperatures: 318, 319, 320, 321, and 322 K. The temperature stability during the isothermal experiments was better than ± 0.1 K, since the crystallization kinetics are very sensitive to temperature (see Fig. 1, below). During the isothermal/isochronal crystallization experiments the storage and loss shear moduli were recorded. The strain amplitude was adjusted so as to avoid

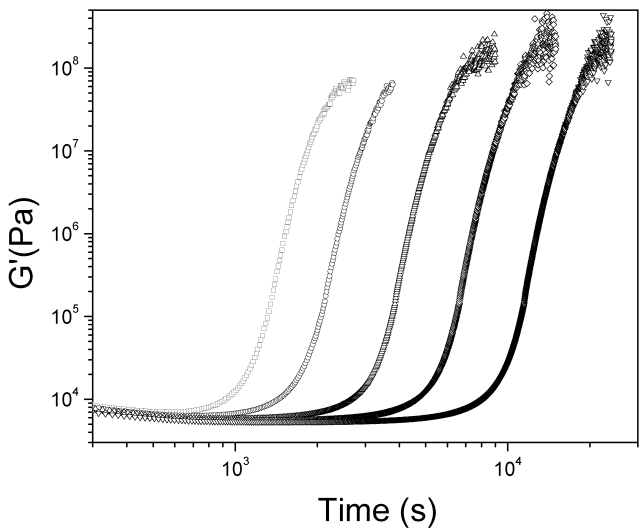

Fig. 1. Time-dependence of the storage moduli during isothermal crystallization for different crystallization temperatures: (□): 318 K, (○): 319 K, (△): 320 K, (◇): 321 K and (▽): 322 K (The corresponding loss moduli data are omitted for clarity (see Fig. 4)). The experiments were performed by cooling from an initial temperature of 353 K to the different crystallization temperatures. The frequency was 1 rad/s and the maximum value of the strain amplitude (which was decreasing during the runs to avoid slip) was 4%.

slip conditions. The subsequent isochronal heating experiments are performed under the same experimental conditions ($\omega = 1$ rad/s, strain amplitude of 4%).

The steady shear experiments were made both with a cone and plate and parallel plate geometry with a gap of about 1 mm. In principle, the inhomogeneous shear rate in the latter experiment can influence the crystallization process. We found that crystallization started from the outer parts of the plates where the largest shear rate exist but the crystallization times were identical for the two geometries investigated. The experiments consisted again of T-jumps from an initial temperature of 353 K to different final crystallization temperatures where we monitored the viscosity for a given shear rate as a function of time. The time where the viscosity value was doubled from its corresponding value in the undercooled melt was taken as the characteristic crystallization time. In an alternative definition the crystallization time was taken as the time required for the system to reach a given viscosity value during the crystallization process. Subsequently, the sample was heated again to 353 K and a new quench was performed to the same crystallization temperature but using a different shear rate. In this way we were able to obtain a series of characteristic crystallization times for the corresponding shear rates.

2.2. Optical microscopy

A Zeiss Axioskop 2 polarizing optical microscope was used together with a Linkam heating stage (THMS 600) and a TP93 temperature programmer (heating and cooling rates of 0.1–90 K/min). We have followed the growth of crystals in real time by a continuous recording using a CCD camera (1/2 in. SONY color camera) and a fast frame grabber (capable of up to 50 frames/s). The analysis in terms of the nucleation density, shape and growth rates was made with an appropriate software (Image Pro Plus). The experiments were made by heating to an initial temperature of 353 K following quenches to different crystallization temperatures.

3. Results and discussion

3.1. Thermal-induced crystallization

The time-dependence of the storage modulus recorded after temperature jumps from an initial temperature above the equilibrium melting temperature to different crystallization temperatures is shown in Fig. 1 (the corresponding data for the loss modulus are omitted for clarity—see Fig. 4, below). The oscillatory experiments have been performed with low strain amplitudes which do not influence the crystallization kinetics. Therefore the isothermal/isochronal experiments reflect solely the thermally-induced crystallization [24]. In a subsequent experiment we performed isochronal heating runs aiming to melt the crystalline structures. The results from these runs for the storage moduli are shown in Fig. 2. The higher the crystallization temperature the higher is the corresponding apparent melting temperature, as indicated by the precipitous drop of the G', reflecting the different lamellae thicknesses at the different crystallization temperatures.

The storage (and loss moduli) of Fig. 1 have an S-shape with short and long-time plateaus describing, respectively, the viscoelastic properties of the undercooled melt and final spherulitic structures. The similarity in the shape of the curves indicates that the crystallization mechanism is an invariant. This is depicted in Fig. 3 where the isochronal/isothermal data sets are shifted with respect to a reference temperature ($T_{ref} = 318$ K) :

$$G^*(t;T) = G^*(b_T t;T_{ref}) \quad (1)$$

According to Eq. (1), at each crystallization temperature a single time-scale shift factor b_T allow superposition of all viscoelastic data at temperature T with the data at the reference temperature T_{ref}. The excellent overlay of the curves—apart from the small differences at short times reflecting the slight differences in the viscoelastic properties of the supercooled melt because of the different crystallization temperatures—is a strong evidence of a uniform crystallization mechanism. The shift factors are plotted in the inset as a function of the crystallization temperature T_c, the degree of supercooling ($\Delta T = T_m^0 - T_c$, where T_m^0 is the equilibrium melting temperature, $T_m^0 = 346$ K) and f is a temperature correction factor ($= 2T_c/(T_m^0 + T_c)$). Assuming spherulitic growth and instantaneous nucleation the Avrami equation [27] for the transformed volume fraction, φ_S, into the spherulites can be employed:

$$\varphi_S(t) = 1 - \exp(-kt^n) \quad (2)$$

where n, the Avrami exponent and k, a rate constant. The

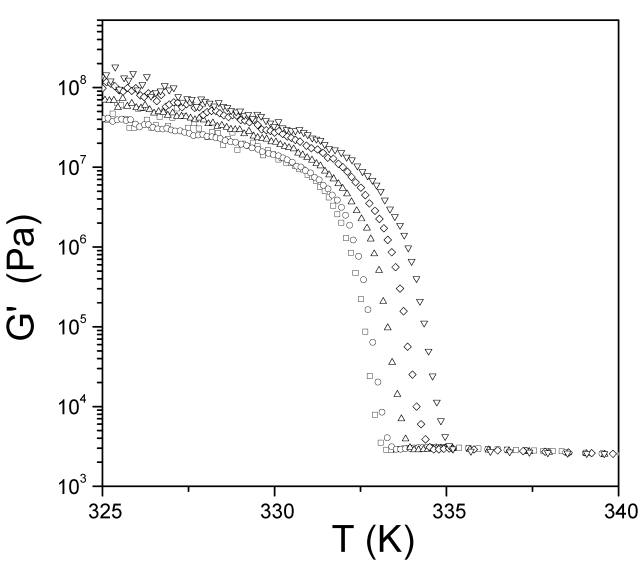

Fig. 2. Isochronal temperature runs following the crystallization kinetics. The symbols are the same as in Fig. 1. Notice the strong dependence of the (apparent) melting temperature on the crystallization temperature.

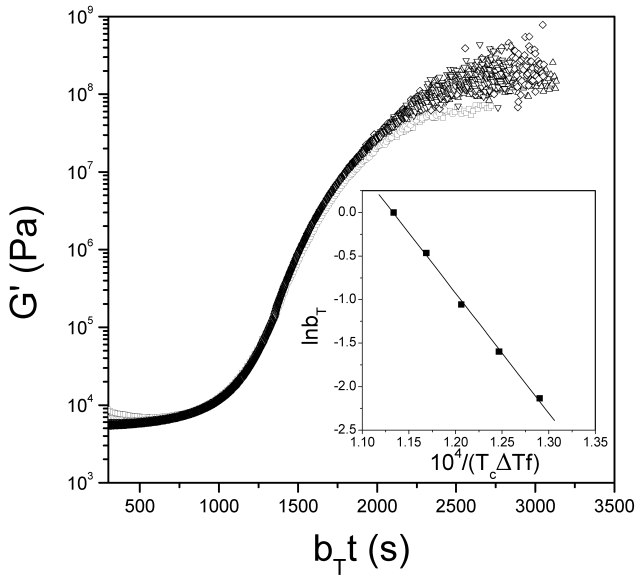

Fig. 3. Time–temperature superposition for the data shown in Fig. 1. The data have been shifted on the horizontal axis by a shift factor b_T which is shown in the inset. The reference temperature was 318 K.

latter (φ_S) can be transformed into the relative degree of crystallinity assuming a constant crystallinity within the spherulites. The Avrami exponent reflects the dimensionality of the growth and the nature of the nucleation and growth process. For example a value of 3 can result either from spherulitic growth from heterogeneous nuclei or from a two-dimensional lamellar growth from homogeneous nuclei. On the other hand, a value of 4 can only result from spherulitic growth and homogeneous nucleation. For spherulites growing from instantaneous (athermal) nuclei, as indicated by the time-resolved microscopy study (see below), we get $n = 3$ and

$$k = \frac{4}{3}\pi N_a R_g^3 \tag{3}$$

where R_g, the growth rate and N_a, the density of activated nuclei. In our experiments N_a can be estimated from the final number density of spherulites $N_{a,\infty}$ in the sample. The characteristic crystallization time, $t_{1/2} = (\ln 2/k)^{1/3}$ is then proportional to the inverse of the growth rate:

$$R_g = \left(\frac{3\ln 2}{4\pi N_a}\right)^{1/3}\frac{1}{t_{1/2}} \tag{4}$$

Since the shape of the shear modulus during crystallization is invariant for the different crystallization temperatures (Fig. 1), $t_{1/2}^{-1}$ can be assumed to be proportional to the shift factor b_T and its temperature dependence can be analyzed in analogy to the growth rates in the theory of Lauritzen and Hoffman [28]. According to the Turnbull and Fisher formalism—devoted to nucleation in metals—the crystal growth rate is, in the simplest form [29]

$$b_T \propto t_{1/2}^{-1} \propto R_g \approx R_0 \exp\left(-\frac{\Delta G_\eta^* + \Delta G^*}{kT}\right) \tag{5}$$

where R_0, the growth rate constant, ΔG_η^*, the activation energy for transport of crystallizing units across the crystal–liquid interface and ΔG^*, the Gibbs free energy required to form a nucleus of critical size on the face of a crystal. In the theory of Lauritzen and Hoffman [28] the first and the second term in the above equation are modified as:

$$R_g(i) \approx \frac{z}{N^v}\exp\left(-\frac{U}{R(T-T_\infty)}\right)\exp\left(-\frac{K_g(i)}{T\Delta Tf}\right) \tag{6}$$

where z, a parameter containing mobility terms, N, the degree of polymerization, and the value of the exponent v depends on the growth regime. The first factor is proportional to the exponential function of the activation energy for the viscous flow U, divided by the temperature excess over the ideal glass transition temperature T_∞ (which is the well-known Vogel–Fulcher–Tammann or the Suzuki–Kovacs equation). The above parameters for PCL are $U = 1500$ cal/mol and $T_\infty = 180$ K [30]. The second factor is related to the nucleation rate constant $K_g(i)$ and contains the heat of fusion, the crystal lateral and fold surface free energies and a numerical factor describing the competition between the rate of deposition of secondary nuclei and the rate of lateral surface spreading. The nucleation rate constant can be estimated from the shift factors plotted in the inset to Fig. 3 ($K_g(i) = 86,400$ K^2) and is in good agreement with literature values for PCL (85,600 K^2) [30] implying that the latter reflect solely thermally-driven crystallization.

The excellent overlay of the curves in Fig. 3 (see above) suggest a uniform crystallization mechanism and similar morphological changes at all crystallization temperatures investigated. Although a detailed model for the time dependence of the shear modulus G^* is not necessary for the present study, we briefly discuss some morphological models which may be responsible for the characteristic S-shape. In Fig. 4, optical micrographs taken during the crystallization process are shown together with the real $G'(t)$ and imaginary part $G''(t)$ of the complex shear modulus. Since in the final state the system is space-filled with spherulites, it is reasonable to assume that the two phase system is composed of spherulites and an amorphous phase. Different models have been proposed to account for the dependence of the volume fraction of the composite modulus G^* (Voigt, Reuss, Kerner, Budiansky, percolation, and gelation models [2,23,25,26]). The upper and lower bounds of these dependencies are given by a 'parallel' model (Voigt)

$$G^* = (1-\varphi_S)G_a^* + \varphi_S G_S^* \tag{7}$$

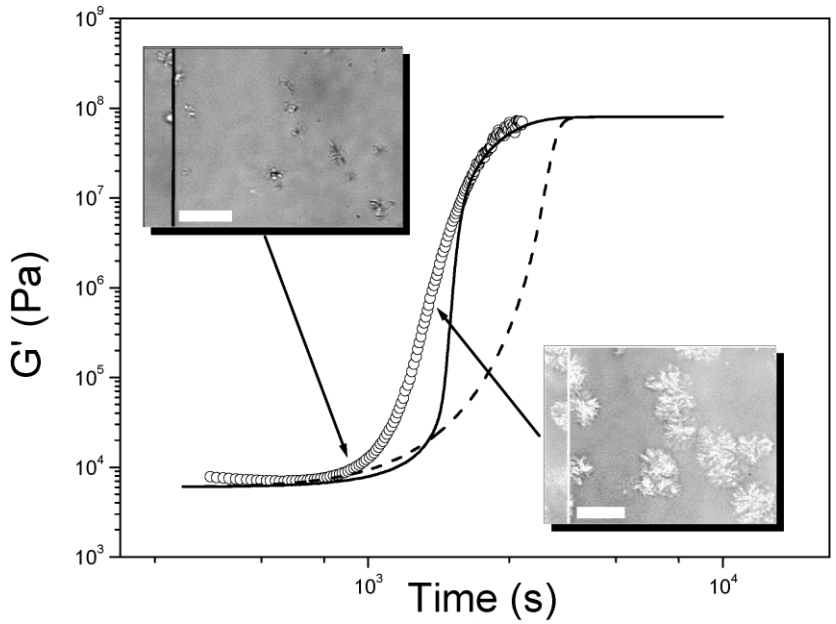

Fig. 4. Time-dependence of the storage (open symbols) and loss (filled symbols) moduli during isothermal crystallization at 318 K. Optical micrographs are shown at selected times as indicated. The micrograph taken at 2560 s corresponds to the time where spherulites impinge. The dashed and solid lines are the results of the $G'(t)$ fits to the Kerner and Budiansky model, respectively. The Avrami parameter in Eq. (2) was set to $n = 3$ (spherulite growth from heterogeneous nuclei) and the moduli of the amorphous $G'_a = 6 \times 10^3$ Pa ($G''_a = 2 \times 10^4$ Pa) and spherulitic phases $G'_S = 8 \times 10^7$ Pa ($G''_S = 1 \times 10^7$ Pa) were taken from the experimental values at $t = 0$ and $t \to \infty$, respectively. The fit to the Kerner model resulted in $k = 2.0 \times 10^{-10}$ and $\gamma = 0.66$. The fit parameters to the Budiansky model were $k = 1.5 \times 10^{-10}$ and $\varepsilon = 0.4$.

and by a 'series' model (Reuss)

$$\frac{1}{G^*} = \frac{(1-\varphi_S)}{G^*_a} + \frac{\varphi_S}{G^*_S} \tag{8}$$

respectively, where φ_S, the volume fraction of spherulites, φ_a ($= 1 - \varphi_S$), the volume fraction of the amorphous phase and G^*_a and G^*_S are the shear moduli of the amorphous and spherulitic phases, respectively. Assuming a constant ratio of amorphous to crystalline component in the spherulite interior during its growth, φ_c, the volume fraction of the crystalline phase can be extracted from φ_S.

A more detailed model for spherical particles included in a matrix is the Kerner model [31]. According to this model the modulus of the composite material is:

$$G^* = G^*_a \frac{\varphi_a G^*_a + (\gamma + \varphi_S) G^*_S}{(1 + \gamma\varphi_S) G^*_a + \gamma\varphi_a G^*_S} \tag{9}$$

where $\gamma = 2(4 - 5\nu)/(7 - 5\nu)$ and ν is Poisson's ratio. Lastly, a model which predicts phase inversion at intermediate compositions was developed by Budiansky [32]:

$$\frac{\varphi_a}{1 + \varepsilon\left(\frac{G^*_a}{G^*} - 1\right)} + \frac{\varphi_S}{1 + \varepsilon\left(\frac{G^*_S}{G^*} - 1\right)} = 1 \tag{10}$$

where $\varepsilon = 2(4 - 5\nu)/15(1 - \nu)$. This model yields a drastic change in the mixing law over the small φ_S range of the phase inversion. The real part of the shear modulus in the Budianski model yields:

$$G' = -\frac{G'_a + G'_S - \varepsilon(G'_a + G'_S) - \varphi_S G'_a - \varphi_a G'_S}{2(\varepsilon - 1)} + \sqrt{\left(\frac{G'_a + G'_S - \varepsilon(G'_a + G'_S) - \varphi_S G'_a - \varphi_a G'_S}{2(\varepsilon - 1)}\right)^2 - \frac{\varepsilon G'_S G'_a}{\varepsilon - 1}} \tag{11}$$

where G'_a and G'_S are the real parts of the shear moduli of the amorphous and spherulitic phases, respectively.

The optical micrographs revealed that already at about 1000 s, there were spherulites present of diameter of some microns (4–5 μm), however, the moduli were insensitive to their presence due to the very small volume fraction. At 1600 s, the moduli start to increase and the spherulites are 10–20 μm in size as shown in the optical micrograph (upper left corner of Fig. 4). These spherulites can still flow within the undercooled melt. At about 2000 s, the spherulites impinge (lower right corner of Fig. 4) and the moduli cross from a liquid-like response at shorter times to a solid-like response at longer times.

Simulated curves using the Kerner (dashed line) and Budiansky morphological models (solid line) are also shown in Fig. 4. For this purpose the Avrami dependence for φ_S (Eq. (2)) was incorporated in the models, with $n = 3$ for spherulitic growth from heterogeneous nuclei. For the parameter k, similar values were chosen in the two models since the same crystallization kinetics are behind. The values

of all parameters, k, γ, ε, G'_a, G''_a, G'_S and G''_S are included in the caption to Fig. 4. Notice, that none of these simple morphological models can describe the evolution of the viscoelastic properties over the entire time range. The optical micrograph indicated isolated spherulites in the initial part of crystallization that may be described by the Kerner model (spheres in a matrix). For the late stages of the crystallization process the Budiansky model (phase inversion) provides a better representation of the modulus.

3.2. Shear-induced crystallization

In order to investigate the influence of shear flow on the crystallization process we have performed experiments at constant rates of shear following quenches from an initial temperature of 353 K to different final crystallization temperatures. A given shear rate was applied immediately following the quench and the viscosity was followed as a function of time. Some typical viscosity curves for different shear rates at a crystallization temperature of 319 K are shown in the inset to Fig. 5 and show an 'incubation' period followed by a strong increase at longer times. The increase in $\eta(t)$ at longer times signifies the onset of crystallization. There is a nice correspondence of the crystallization times obtained from the dynamic and low shear rate steady experiments: in the steady shear experiment of Fig. 5 (inset) at the lowest shear rate the crystallization sets in at about 2000 s, which is exactly the time obtained from the oscillatory shear experiment (Fig. 1) at the same temperature (319 K). This signifies that a shear rate of 0.025 s^{-1} does not influence the crystallization process. Increasing shear rate reduces the incubation period in $\eta(t)$ and speeds-up the crystallization process but the overall $\eta(t)$ dependence is invariant. We point-out here that the shear rates employed in the present study are 5–400 times lower than in the previous rheological investigation [21]. Despite this, we still observe an enhanced crystallization process meaning that even such low deformations are adequate to speed-up the process with implication in processing (i.e. injection moulding).

From such $\eta(t)$ dependencies we define an operational crystallization time (t_c) as the time required for the viscosity to double its initial value. As an alternative definition we have used the time needed for the viscosity to obtain a certain value (i.e. 3×10^4 Pa s). The thus obtained, admittedly operational crystallization times, are plotted in Fig. 5 as a function of the shear rate and the good agreement results from the invariant $\eta(t)$ dependence. Therefore, independent from the t_c definition, increasing shear rate speeds-up the crystallization process. At the highest shear rate employed here—the upper value determined by slip conditions—the characteristic times are reduced by nearly one decade. Such speed-up of the crystallization process has been observed before, and here we try to quantitatively account for it.

The experimentally found $t_c(\dot{\gamma})$ dependence can be understood in terms of the partial orientation and extension of the chains in the strained melt. It is conceivable that the transition from the melt to the crystal will be modified because of the different enthalpy and entropy of the strained melt with respect to the fully relaxed (unstrained) melt [33]. The decrease in the enthalpy by the applied mechanical force $\delta H_m(\dot{\gamma})$ is a consequence of better packing, which reduces the distance between the chains, and due to chain

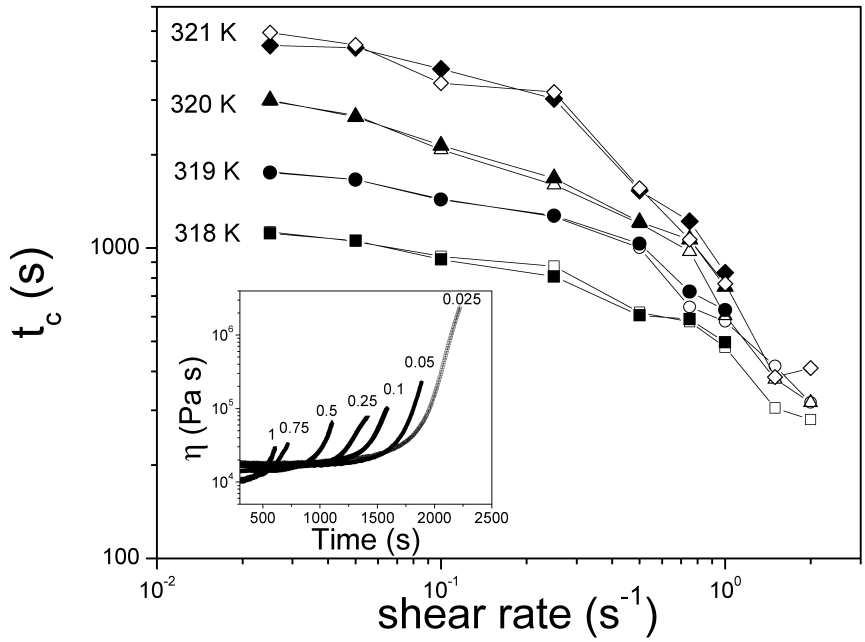

Fig. 5. Crystallization times obtained at different temperatures as indicated plotted as a function of the shear rate. The open and filled symbols correspond to the different definitions of the crystallization time (see text). In the inset the time-evolution of the viscosity is shown at $T = 319$ K for different shear rates as indicated.

extension, which increases the number of lower energy conformations (mostly from *gauche* to *trans*). At the same time, the entropy decreases by $\delta S_m(\dot{\gamma})$ as a consequence of the reduction of the available conformations with chain extension and orientation and as a consequence of the reversible enthalpy reduction ($\delta H_m(\dot{\gamma})/T$). Consequently, the strain applied to a melt at any temperature increases its free enthalpy according to: $G_m(\dot{\gamma}, T) - G_m(\dot{\gamma} = 0, T) = \delta H_m(\dot{\gamma}) - T\delta S_m(\dot{\gamma}) > 0$. This increase will result in the increase in the equilibrium melting temperature of the strained system as compared to the unstrained situation as long as $T < T_m$, since [33]

$$T_m(\dot{\gamma}) = \frac{\Delta H(\dot{\gamma} = 0) - \delta H_m(\dot{\gamma})}{\Delta S(\dot{\gamma} = 0) - \delta S_m(\dot{\gamma})} = T_m(\dot{\gamma} = 0)\frac{1 - \delta H_m(\dot{\gamma})/\Delta H(\dot{\gamma} = 0)}{1 - (T_m(\dot{\gamma} = 0)/T)\delta H_m(\dot{\gamma})/\Delta H(\dot{\gamma} = 0)} \quad (12)$$

There are some experimental reports [10] and theoretical arguments [5] claiming the increase in the equilibrium melting temperature in the strained system. For example an increase in the equilibrium melting temperature under shear flow was calculated based on the first normal stress difference [5]. This problem, however, requires further investigations. Furthermore, the formal introduction of Eq. (12) into Eq. (6) may lead to several difficulties and the way the shear field may influence the size of the primary and secondary nuclei, the crystal characteristics (σ, σ_e) and the enthalpy of fusion are not known.

In order to avoid these difficulties [12,34] we reduce our data analysis to some simple assumption on the origin of the crystal growth under shear. As in the case of thermally-induced crystallization, we assume that shear-induced crystallization consists in three-dimensional growth (justified by the spherulites in the optical micrographs) starting from pseudo-instantaneous (see below) nuclei. Our optical microscopy experiments have shown a 30-fold increase in the nucleation density in the strained as compared to the unstrained melt [22], which is a clear indication that the nucleation density is strongly affected by the shear flow. The molecular origin for this increase is the elongation and orientation of parts of the polymer chains (segments) in the sheared melt. This pre-ordered regions act as precursors for the nucleation. It is known (see e.g. [12]) that the shear-induced nucleation (which is in our case is an instantaneous process) can be a fast process as compared to the crystal growth detected in rheology; i.e. that the final nucleation density (saturation for the given shear rate and temperature) is reached during shear-induced crystallization well before a considerable increase in the shear modulus can be detected. We will call that 'pseudo-instantaneous shear-induced nucleation'. Under this premise (that the density of activated nuclei N_a is almost constant during spherulitic growth), Eq. (3) holds also for the shear induced-crystallization. Then, for a given number of active nuclei the growth rate is inversely proportional to the characteristic crystallization time. In our shear-induced crystallization experiments, $t_{1/2}$ can be replaced by $t_c(\dot{\gamma})$ in Eq. (4). Under these assumptions the shear rate dependence of the nucleation density N_a would lead to an increase in the growth rate without changing the growth mechanism. Eq. (5) should therefore also hold for $t_c(\dot{\gamma})$ instead of $t_{1/2}$. With this rather strong assumption the observed decrease in experimentally observed characteristic times with increasing shear rate has to be related to the increase in the number of active nuclei and an increase in the growth rate due to preordered regions of the melt. In literature there are some reports, however, claiming the enhancement of the growth rate [13] for high shear rates. In order to fully justify our assumptions on nucleation density and growth rate under shear in situ optical microscopy experiments are needed.

As discussed above for the shear-induced nucleation the molecular origin of the increase of growth rate with shear rate $\dot{\gamma}$ is related to an orientation and stretching of chain segments in the melt, which would lead to a decrease in the melt entropyS_m. Since an extension of the classical theory of nucleation and growth to shear-induced crystallization needs a large number of parameters such as the shear rate dependence of melting temperature, heat of fusion, surface tension, etc. we reduce our discussion to a simple kinetic model based on reaction rate theory (see Scheme 1).

We assume that for crystal growth (e.g. by secondary nucleation) the system has to overcome an activation barrier Δg^*, which is the Gibbs free energy required to form a locally preordered melt region (stretched and oriented chain segments or critical nuclei) on the face of a growing crystal. In this picture the value of the free enthalpy G^* for the activated (transient) melt state or nucleus of critical size is expected to be independent of the shear rate. In other words, the free enthalpies of the preordered regions (or critical

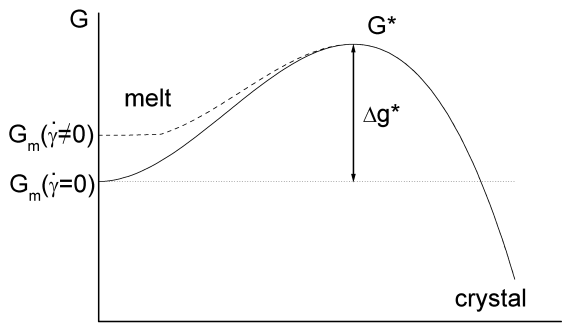

Scheme 1. Free enthalpy of the unstrained (solid line) and strained liquid (dotted line) and free enthalpy barrier Δg^* required for the formation of an activated melt state (e.g. elongated and oriented chains or secondary nucleus of critical size).

nuclei) without shear are not different from those formed under shear (which is probably correct under low shear deformations). G^* is expected to be mainly of enthalpic origin (e.g. due to conformational changes necessary to form stretched chain segments). For the assumption of crystal growth by secondary nucleation on the growing crystal surface the total energy of a critical nucleus of a given size is expected to depend only on the surface energy and the heat of fusion. The activation barrier Δg^* is then defined as $\Delta g^* = G^* - G_m$, where G_m is the free enthalpy of the melt. Under these assumptions the growth rate in the presence of external shear can be expressed by Eq. (5) replacing ΔG^* in the second term by $\Delta g^*(\dot\gamma)$. The first factor is expected to be identical to the corresponding transport term in Eq. (6). Then, we get for the crystal growth rate under shear:

$$t_c(\dot\gamma)^{-1} \propto R_g(\dot\gamma, T) \propto \exp\left(-\frac{U}{R(T - T_\infty)}\right) \exp\left(-\frac{\Delta g^*(\dot\gamma, T)}{RT}\right) \quad (13)$$

with the free enthalpy barrier $\Delta g^*(\dot\gamma)$ to form a precursor for the nucleation or the formation of a nucleus of critical size in the strained melt. The free enthalpy of a melt under shear $G_m(\dot\gamma, T)$ is expected to exceed the corresponding value of the relaxed melt $G_m(\dot\gamma = 0, T)$ by $\delta G_m(\dot\gamma, T) = G_m(\dot\gamma, T) - G_m(\dot\gamma = 0, T) > 0$ (see Scheme 1). Since for low shear rates the contribution of conformational changes to $G_m(\dot\gamma)$ is expected to be small, we will consider the changes in melt entropy $\delta S_m(\dot\gamma)$ to be dominant as compared to the small contributions in $\delta H_m(\dot\gamma)$. With the assumption that the free enthalpy of the activated stage G^* (e.g. the total free enthalpy of stretched and oriented regions of the chain or of a stable nucleus) remains almost constant, the barrier $\Delta g^*(\dot\gamma)$ is expected to decrease under shear since the entropy of the melt is a decreasing function of shear($\delta S_m(\dot\gamma) < 0$) :

$$\Delta g^*(\dot\gamma \neq 0) = \Delta g^*(\dot\gamma = 0, T) - [G_m(\dot\gamma \neq 0, T) - G_m(\dot\gamma = 0, T)] \cong \Delta g^*(\dot\gamma = 0, T) + T\delta S_m(\dot\gamma) \quad (14)$$

Assuming that the characteristic time derived from the viscosity curves is proportional to the inverse nucleation rate ($t_c^{-1} \propto R_n$), then the $\ln t_c - U/R(T_c - T_\infty)$ versus T^{-1} plot yields directly the free enthalpy barrier Δg^* for nucleation. Knowledge of $\Delta g^*(\dot\gamma)$ and $\Delta g^*(\dot\gamma = 0)$ allows calculating $\delta G_m(\dot\gamma, T) = G_m(\dot\gamma, T) - G_m(\dot\gamma = 0, T)$ using Eq. (14).

These dependencies for different values of $\dot\gamma$ are shown in Fig. 6. Within the investigated temperature range the nucleation rate strongly increases with decreasing temperature. Furthermore, there is pronounced shear rate dependence: the higher the shear rate the smaller is the slope. At the highest shear rate shown ($\dot\gamma = 1\ s^{-1}$) the dependence becomes relatively flat and the nuclei are activated by the shear flow rather than by the thermal fluctuations. Therefore one can assume that the shear stress generates a large number of nuclei that leads to a shear induced 'pseudo heterogeneous nucleation'. From the low value of the free enthalpy barrier for $\dot\gamma = 1\ s^{-1}$ one can conclude that the number of nuclei created by shear is close to saturation. This is in agreement with the increase in the nucleation density found in optical microscopy. The activation barrier for thermally activated (nearly static conditions: $\dot\gamma = 0.025\ s^{-1}$) nuclei is about 450 kJ/mol and is reduced to 170 kJ/mol at $1\ s^{-1}$. Therefore a shear rate of $\dot\gamma \approx 2\ s^{-1}$ reduces the activation barrier for the formation of stable nuclei practically to zero.

Assuming that a shear rate of about $1\ s^{-1}$ results in a nucleation of all possible nuclei it is worth estimating the chain deformation related to this shear rate. In the estimation we assumed that the relaxation of chain after a shear deformation follows a simple Debye relaxation, i.e. $\phi = \exp(-t/\tau)$ and that the superposition principle is fulfilled, i.e. $\gamma = \int_{-\infty}^{t} \phi(t - t')\dot\gamma(t')dt'$. For the steady state ($\dot\gamma(t) = \dot\gamma_0 = \text{const}$) one gets $\gamma(t) = \dot\gamma_0\tau$. With the assumption that the characteristic relaxation time for the flow relaxation can be defined by the condition $G'(\omega) = G''(\omega)$. From frequency dependent rheological experiments in the melt, directly after the quench to the final crystallization temperature, we estimate an experimental value for τ of 0.1 from the crossing point of $G'(\omega)$ and $G''(\omega)$. With $\dot\gamma_0 \cong 0.01\ldots2\ s^{-1}$ one gets $\gamma(t) \cong 0.001\ldots0.2$. If one assumes that a sphere will be deformed in a shear field to an ellipsoid the main axes deform by $1 - \sin\gamma$ and $1 + \sin\gamma$ which yields a ratio of length (L) to thickness (B) of the ellipsoid of $L/B = 1 + 2\gamma + 2\gamma^2 + 5/9\gamma^3$ and $L/L_0 = 1 + \gamma + \gamma^3/6$ and L_0 is the unperturbed length. This leads to a maximum of about 10% stretching of the coil for our experiments. The low level of chain deformation is suggestive of a small number

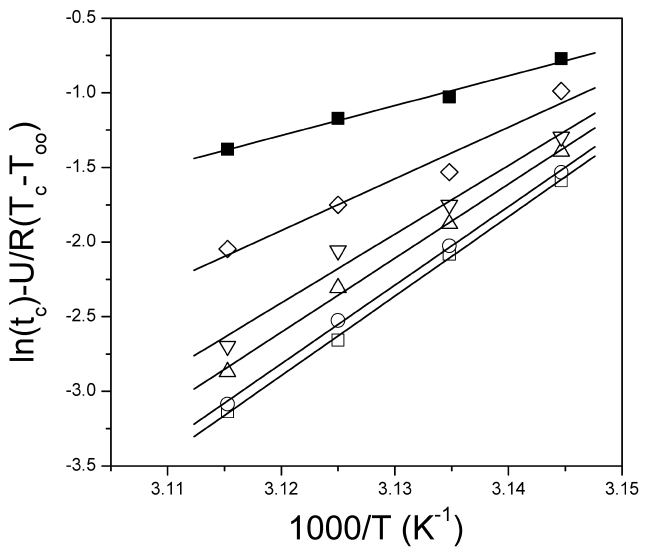

Fig. 6. Characteristic crystallization times plotted versus inverse temperature for different shear rates: (□): 0.025, (○): 0.05, (△): 0.1, (▽): 0.25, (◇): 0.5 and (■): $1\ s^{-1}$. The lines are linear fits to the data.

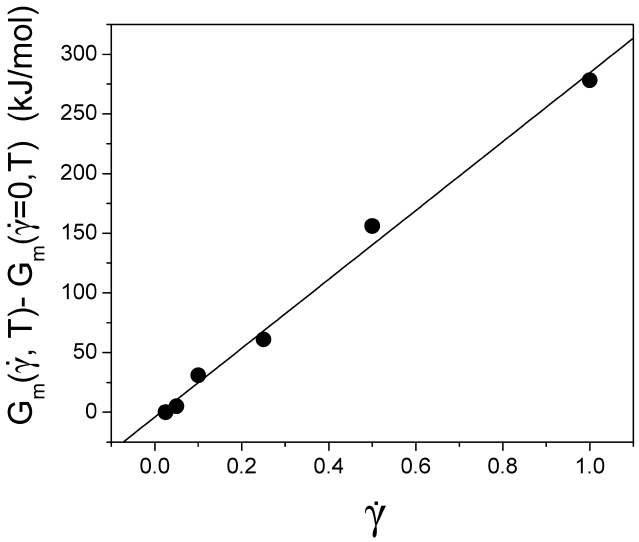

Fig. 7. Shear rate dependence of the free enthalpy difference between the strained and unstrained melt. The line through the data points is the result of a linear fit. Scheme 1 gives the free enthalpy map.

of *gauche* to *trans* conformational transitions which act as precursors for the nuclei formation.

In Fig. 7 the additional contribution to the free enthalpy $\delta G_m(\dot\gamma, T) = G_m(\dot\gamma, T) - G_m(\dot\gamma = 0, T)$ due to the shear is plotted as a function of shear rate $\dot\gamma$. Within the investigated interval the increase in δG_m with $\dot\gamma$ is linear. Assuming that the main effect of chain extension is of entropic origin then one can write $\delta G_m \approx -T\delta S_m(\dot\gamma)$. Under this premise, the slope in Fig. 7 is suggestive of a simple linear dependence of the entropy change on the shear strain, i.e. $\delta S_m(\dot\gamma) = S_m(0) - S_m(\dot\gamma) \propto \dot\gamma$. However, the entropy of a chain at fixed elongation is given by [35]:

$$S(\vec{r}) = S(0) - \frac{3}{2}\frac{r^2}{\langle r^2\rangle_0} \tag{15}$$

where $S(0)$ is the entropy and $\langle r^2\rangle_0$ is the mean-squared end-to-end distance of an undisturbed chain (no elongation). If we introduce the known dependence of $\langle r^2\rangle$ on the shear rate, i.e. $\langle r^2\rangle \sim \dot\gamma^2$, derived from Rouse theory [7], into the ensemble averaged entropy $\langle S\rangle$ then we obtain that, $\langle S(r)\rangle \sim \dot\gamma^2$, which contrasts the experimental result shown in Fig. 7. There can be three possible causes for this discrepancy: (a) the contribution from non-negligible enthalpic contributions to δG_m, (b) a different shear rate dependence for the oriented chain segments acting as the precursors for the initial nuclei or (c) the fact that the present polymer is well above the entanglement molecular weight. At present we cannot exclude one of the above possibilities but it would be of interest to derive an exact relation between the *local* entropy of the oriented segments giving rise to the initial nuclei in dependence to the shear rate. However, for a full justification of our rather strong assumptions on the influence of shear on nucleation and growth in situ optical experiments are needed.

3.3. Interrelation between thermal and shear-induced crystallization

Returning to the temperature and shear rate dependence of the characteristic times in Fig. 5, we suggest a rather empirical analysis of the data aiming at obtaining a scaling law for the two types of crystallization experiments. The characteristic crystallization times t_c for the lowest shear rate (i.e. 0.025 s^{-1}) reflect solely thermally-induced crystallization. Thus the curves have been shifted vertically with the shift factors (b_T) shown in the inset to Fig. 3, reflecting the thermally-induced crystallization process. Subsequently, the resulted curves have been shifted along the horizontal axis according to:

$$t_c(\dot\gamma; T) = b_T t_c(\alpha_T \dot\gamma; T_{ref}) \tag{16}$$

The resulted master curve is shown in Fig. 8 and reveals that at each temperature, a single shear-rate scale shift factor α_T (corresponding to the shear-induced crystallization) and a single time-scale shift factor b_T (corresponding to thermal crystallization) allow the superposition of all crystallization times at a given crystallization temperature with the data at the reference temperature (T_{ref} = 318 K). The superposition suggests that, at the low shear rates employed here, there is an underlying law. The data can be fitted satisfactory to an empirical function:

$$b_T t_c = A \exp\left(-\left(\frac{a_T\dot\gamma}{\dot\gamma_0}\right)^n\right) \tag{17}$$

where A = 1331, γ_0 = 1.11 s^{-1} and n = 0.5. The horizontal

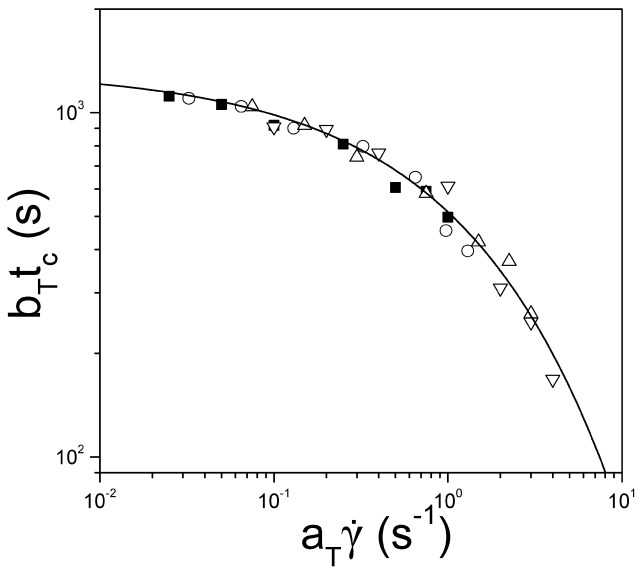

Fig. 8. Superposition of the data sets shown in Fig. 5. The superposition was made first by applying a vertical shift factor b_T (from the T-dependence of Fig. 3) and consequently a horizontal shift factor a_T. The line is a fit to Eq. (16).

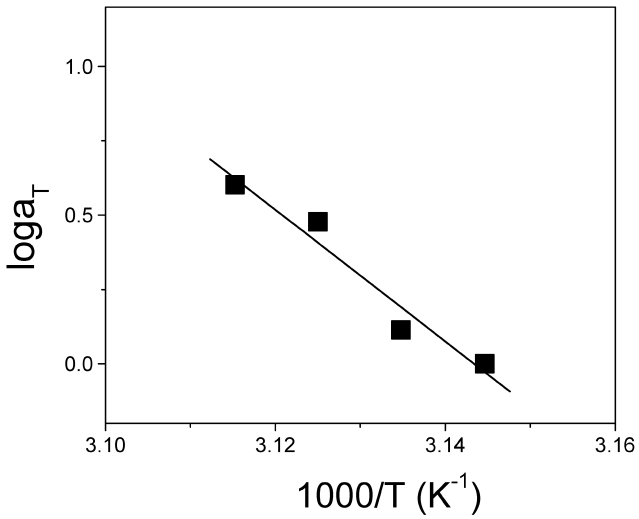

Fig. 9. Horizontal shift factors from Fig. 8, plotted in an Arrhenius representation. The line is the result of a linear fit with an apparent activation energy of 430 kJ/mol.

shift factors are plotted in Fig. 9 and display an Arrhenius temperature dependence within the (small) temperature interval investigated with an apparent activation energy of about 430 kJ/mol. Notice that this activation energy reflects the effect of shear and is of the order of the activation barrier. The master curve implies that the system obeys the shear rate—temperature—superposition principle implying that decreasing temperature and increasing shear rate produce a similar effect on the crystallization times. The effect has been explored here in the limit of low shear rates. It would be of interest to explore the effect of higher shear rates, relevant to polymer processing. Furthermore, since both the shear rate dependence of nucleation density and the shear rate dependence of crystal growth interfere, more detailed experimental and theoretical investigations are necessary for a molecular understanding of such a behavior through a suitable model.

4. Conclusions

We have investigated the crystallization under low shear rates of PCL using rheology and optical microscopy. In the limit of low shear rates it was possible to perform a qualitative analysis of the thermally induced crystallization. We found that a single morphological model of the composite material cannot account for the evolution of the viscoelastic properties over the entire crystallization process. However, the characteristic times and/or shift factors are sufficient to estimate thermodynamic parameters of the crystallization kinetics.

The influence of shear flow on the initial nuclei formation under low shear rates was investigated in steady shear experiments. From measurements of the evolution of the shear viscosity following temperature jumps from the liquid state at different shear rates, the characteristic crystallization times t_c were estimated as a function of crystallization temperature and shear rate. From the shear rate and temperature dependence of the crystallization times we were able (with some assumptions on the crystallization mechanism under shear) to derive the shear rate dependence of the free enthalpy barrier and consequently the free enthalpy difference $\delta G_m(\dot{\gamma}, T) = G_m(\dot{\gamma}, T) - G_m(\dot{\gamma} = 0, T)$. The latter displays a linear dependence on shear rate that can be rationalized by changes in the entropy of the melt state due to coil deformation. Lastly, the temperature and shear rate dependence of the characteristic crystallization times t_c, could be summarized in a 'master plot' indicating the validity of the shear rate—temperature—superposition implying that decreasing temperature and increasing shear rate affect the crystallization times in a universal way.

Acknowledgements

This work was supported by the Greek Secretariat for Research and Technology (GGET) by a grant (PENED2001) and by the Alexander von Humboldt Stiftung. The support of the European Science Foundation in the SUPERNET program and the Fonds der Chemischen Industrie is gratefully acknowledged.

References

[1] Wunderlich B. Macromolecular physics. New York: Academic Press; 1976.
[2] Pogodina NV, Winter HH, Srivinas S. J Polym Sci, Part B: Polym Phys 1999;37:3512–9.
[3] Kornfield J, Kumaraswamy G, Issaian AM. Ind Engng Chem Res 2002;41:6383–92.
[4] McHugh AJ, Spevacek JA. J Polym Sci, Polym Phys Ed 1991;29:969.
[5] Eder G, Janeshitz-Kriegl H, Liedauer S. Prog Polym Sci 1990;15:629.
[6] Eder G. Mater Sci Technol 1997;18:270.
[7] Carl W, Bruns W. Macromol Theory Simul 1994;3:295–303.
[8] Ziabicki A, Alfonso GC. Macromol Symp 2002;185:211–31.
[9] (a) Haas TW, Maxwell B. Polym Engng Sci 1969;9:225. (b) Lagasse RR, Maxwell B. Polym Engng Sci 1976;16:189.
[10] Monasse B. J Mater Sci 1995;30:5002.
[11] Wolkowitz MD. J Polym Sci, Polym Symp 1978;63:365.
[12] Tribout C, Monasse B, Haudin JM. Colloid Polym Sci 1996;274:197.
[13] Duplay C, Monasse B, Haudin JM, Costa JL. Polym Int 1999;48:320.
[14] Jerschow P, Janeschitz-Kriegl H. Int Polym Proc 1997;1:72.
[15] Liedauer S, Eder G, Janeschitz-Kriegl H, Jerschow P, Geymayer W, Ingolic E. Int Polym Proc 1993;3:236.
[16] Kumaraswamy G, Issaian AM, Kornfield JA. Macromolecules 1999; 32:7537.
[17] Koscher E, Fulchiron R. Polymer 2002;43:6931–42.
[18] Sherwood CH, Price FP, Stein RS. J Polym Sci, Polym Symp 1978;63: 77.
[19] Chien MC, Weiss RA. Polym Engng Sci 1988;28:6.
[20] Zhao Y, Keroack P, Prud homme R. Macromolecules 1999;32:1218.
[21] Vleeshouwers S, Meijer HEH. Rheol Acta 1996;35:391.

[22] Floudas G, Hilliou L, Lellinger D, Alig I. Macromolecules 2000;33:6466.
[23] Boutahar J, Carrot C, Guillet J. Macromolecules 1998;31:1921.
[24] Floudas G, Tsitsilianis C. Macromolecules 1997;30:4381.
[25] Alig I, Tadjbakhsch S, Floudas G, Tsitsilianis C. Macromolecules 1998;31:6917.
[26] Alig I, Tadjbakhsch S. J Polym Sci, Polym Phys Ed 1998;36:2949.
[27] (a) Avrami MJ. J Chem Phys 1939;7:1103. (b) Avrami MJ. J Chem Phys 1940;8:212. (c) Avrami MJ. J Chem Phys 1941;9:177.
[28] Lauritzen JI, Hoffman JD. J Res Natl Bur Stand 1960;64A:63.
[29] Turnbull D, Fisher JC. J Chem Phys 1949;17:1971.
[30] Floudas G, Reiter G, Lambert O, Dumas P. Macromolecules 1998;31:7279.
[31] Kerner EH. Proc Phys Soc, London 1956;B69:809.
[32] Budiansky B. J Mech Phys Solids 1965;13:223.
[33] Peterlin A. In: Miller RL, editor. Flow induced crystallization. New York: Gordon; 1979.
[34] Gaylor RJ. In: Miller RL, editor. Flow induced crystallization. New York: Gordon; 1979.
[35] de Gennes P-G. Scaling concepts in polymer physics. Ithaca: Cornell University Press; 1979.